Neuroprotective effects of fatty acid amide hydrolase catabolic enzyme inhibition in a HIV-1 Tat model of neuroAIDS

Douglas J. Hermes[a], **Changqing Xu**[a], **Justin L. Poklis**[b], **Micah J. Niphakis**[c], **Benjamin F. Cravatt**[c], **Ken Mackie**[d], **Aron H. Lichtman**[b], **Bogna M. Ignatowska-Jankowska**[e], and **Sylvia Fitting**[a]

[a]Department of Psychology & Neuroscience, University of North Carolina at Chapel Hill, Chapel Hill, NC 27599, USA

[b]Department of Pharmacology & Toxicology, Virginia Commonwealth University, Richmond, VA 23298, USA

[c]Department of Chemical Physiology, Scripps Research Institute, La Jolla, CA 92037, USA

[d]Department of Psychological & Brain Science, Indiana University, Bloomington, IN 47405, USA

[e]Okinawa Institute of Science and Technology, Neuronal Rhythms in Movement Unit, Okinawa 904-0495, Japan

Abstract

The HIV-1 transactivator of transcription (Tat) is a neurotoxin involved in the pathogenesis of HIV-1 associated neurocognitive disorders (HAND). The neurotoxic effects of Tat are mediated directly via AMPA/NMDA receptor activity and indirectly through neuroinflammatory signaling in glia. Emerging strategies in the development of neuroprotective agents involve the modulation of the endocannabinoid system. A major endocannabinoid, anandamide (N-arachidonoylethanolamine, AEA), is metabolized by fatty acid amide hydrolase (FAAH). Here we demonstrate using a murine prefrontal cortex primary culture model that the inhibition of FAAH, using PF3845, attenuates Tatmediated increases in intracellular calcium, neuronal death, and dendritic degeneration via cannabinoid receptors (CB_1R and CB_2R). Live cell imaging was used to assess Tat-mediated increases in $[Ca^{2+}]_i$, which was significantly reduced by PF3845. A time-lapse assay revealed that Tat potentiates cell death while PF3845 blocks this effect. Additionally PF3845 blocked the Tatmediated increase in activated caspase-3 (apoptotic marker) positive neurons. Dendritic degeneration was characterized by analyzing stained dendritic processes using Imaris and Tat was found to significantly decrease the size of processes while PF3845 inhibited this effect. Incubation with CB_1R and CB_2R antagonists (SR141716A and AM630) revealed that PF3845-mediated calcium effects were dependent on CB_1R, while reduced neuronal death and

degeneration was CB_2R-mediated. PF3845 application led to increased levels of AEA, suggesting the observed effects are likely a result of increased endocannabinoid signaling at CB_1R/CB_2R. Our findings suggest that modulation of the endogenous cannabinoid system through inhibition of FAAH may be beneficial in treatment of HAND.

Keywords

cannabinoids; anandamide; HIV-1 Tat; neurodegeneration; neuroprotection

1. Introduction

Combination antiretroviral therapy (cART) has greatly improved the life expectancy of patients infected with human immunodeficiency virus 1 (HIV-1), however many still exhibit mild neurocognitive deficits referred to as HIV-1 associated neurocognitive disorders (HAND) (Sacktor et al., 2002; Gannon et al., 2011; Heaton et al., 2011). Severity of HAND symptoms strongly correlates with synaptodendritic damage, such as dendritic simplification, axonal disruption, and synaptic loss (Masliah et al., 1997; Ellis et al., 2007). The HIV-1 transactivator of transcription (Tat) protein, a neurotoxin that likely plays a major role in the pathogenesis of HAND (Rappaport et al., 1999; King et al., 2006; Rao et al., 2014; Carroll and Brew, 2017), directly disrupts healthy neuronal function by dysregulating the AMPA/NMDA receptor system leading to increased intracellular $[Na^+]_i$ and $[Ca^{2+}]_i$ causing mitochondrial instability, enhanced cellular excitability, and swelling and/or loss of functional dendritic structures (Cheng et al., 1998; Haughey et al., 2001; Prendergast et al., 2002; Behnisch et al., 2004; Longordo et al., 2006; Brailoiu et al., 2008b; Zucchini et al., 2013; Bertrand et al., 2014; Fitting et al., 2014). Moreover, Tat promotes neuroinflammatory signaling (Nath et al., 1999; Sheng et al., 2000; Hahn et al., 2010; Zou et al., 2011; Jin et al., 2012), which may be a major component of HAND pathogenesis (Mattson et al., 2005; Gannon et al., 2011; Harezlak et al., 2011). The persistence of HAND in the era of cART provokes questions about the causes and treatment of HIV-1-related brain disorders and whether cognitive deficits are reversible (Ellis et al., 2007). Endogenous cannabinoid ligands N-arachidonoylethanolamine (anandamide/AEA) and 2-arachidonoylglycerol (2-AG) have neuroprotective properties that likely play a role in several neurological disorders, including Parkinson's and Alzheimer's diseases (Scotter et al., 2010; Pertwee, 2014). AEA and 2-AG primarily target cannabinoid type 1 receptors (CB_1Rs) and cannabinoid type 2 receptors (CB_2Rs) and are preferentially degraded by fatty acid amide hydrolase (FAAH) and monoacylglycerol lipase (MAGL), respectively. Neuronal CB_1R activation offers neuroprotection by limiting the synaptic release of glutamate (Marsicano et al., 2003; Chevaleyre et al., 2006; Rossi et al., 2011; Chiarlone et al., 2014) and downregulating N-methyl-D-aspartate (NMDA) receptor activity (Derkinderen et al., 2003; Marsicano et al., 2003; Liu et al., 2009; Li et al., 2010; Hampson et al., 2011; Sanchez-Blazquez et al., 2014). Psychoactive side effects including sensorimotor, affective, and cognitive disturbances limit the therapeutic utility of CB_1R agonists (Di Marzo, 2008). Further, direct application of AEA and 2-AG have poor clinical viability because their rapid degradation. Despite the neuroprotective and anti-inflammatory potential of endogenous cannabinoid hydrolytic enzyme inhibitors, they have not been evaluated evaluated in models of the neuro-acquired

immune deficiency syndrome (neuroAIDS). Strong preclinical evidence shows that selective inhibitors of FAAH and MAGL ameliorate neurodegenerative disease processes in a variety of different animal models (Naidoo et al., 2011; Pertwee, 2014). Hydrolytic enzyme inhibitors, such as the FAAH inhibitor PF3845, show high selectivity and potency with minimal side effects (Ahn et al., 2009; Booker et al., 2012; Niphakis et al., 2013). Specifically, PF3845 increases neuronal survival, and elicits antinociceptive and anti-inflammatory effects in mice without cannabimimetic side effects (Booker et al., 2012; Tchantchou et al., 2014).

The goals of this study were to test whether PF3845 produces neuroprotective effects in murine prefrontal cortex (PFC)-derived neuronal cultures challenged with neurotoxic concentrations of Tat, and to identify specific CBRs and potential mechanisms involved in neuroprotection. By conducting live cell $[Ca^{2+}]_i$ imaging studies, time-lapse cell survival assays, and immunocytochemistry it was demonstrated that challenging cultured PFC neurons with Tat significantly increases neuronal $[Ca^{2+}]_i$ levels, decreases neuron survival, and induces loss of dendrite structure, while preincubating cells with PF3845 ameliorates these conditions via CB_1R and CB_2R-related mechanisms.

2. Material and Methods

2.1 Experimental design and statistical analyses

The design of each experiment is detailed in methods provided for each experiment, including the between-subjects factors and a full description of critical variables required for independent replication.

2.2 Treatments

Neurons were treated with HIV-1 Tat_{1-86} (10–500 nM; ImmunoDiagnostics; clade 267 B), PF3845 (10–100 nM, Dr. Benjamin Cravatt), CB_1R antagonist SR141716A (SR1, 50 nM, Tocris, Ellisville, MO) and the CB_2R antagonist AM630 (50 nM, Tocris, Ellisville, MO). Concentrations of PF3845 were chosen based on preliminary experiments (data not shown) and previous studies that assessed the activities of these drugs *in vitro* (Ahn et al., 2009; Niphakis et al., 2013). Tat concentrations in the 10–500 nM range were selected as these concentrations recapitulate the cellular deficits found in individuals with HIV-1 mediated pathology (Kruman et al., 1998; El-Hage et al., 2008; Perry et al., 2010; El-Hage et al., 2011). For all experiments PF3845 was added 30 min prior to experiment start. Tat was added for calcium imaging 1 min after the experiment started and for neuronal survival and dendrite morphology assessments at the beginning of experimental studies. In order to determine the contribution of CB_1R and/or CB_2R activity to observed neuroprotective effects, cultures were incubated with SR1 or AM630 30 min prior to PF3845 treatment and were present throughout the duration of the experiment. Antagonist drug concentrations were chosen to maximally block treatments based on preliminary explorative assessments conducted prior to the main experiments.

2.3 Primary neuronal cultures

All experiments were approved by the University of North Carolina at Chapel Hill and conducted in accordance with the NIH Guide for the Care and Use of Laboratory Animals. Primary neuronal cultures were derived from dissociated PFC of embryonic day 15–16 C57BL/6J mice as previously described (Xu et al., 2017). Collected tissue was minced and incubated (30 min, 37 °C) with trypsin (2.5 mg/ml) and DNase (0.015 mg/ml) in neurobasal medium (Invitrogen) supplemented with B27 (Invitrogen), L-glutamine (0.5 mM; Invitrogen), glutamate (25 mM; Sigma-Aldrich) and an antibiotic mixture (Invitrogen). Tissues were triturated, filtered twice through 70 μm pore nylon mesh and then plated on MatTek 35 mm glass bottom dishes (1×10^5 cells per dish, for calcium imaging), on coverslips (2×10^5 cells per coverslip, for immunocytochemistry), and on 12-well plates (2×10^5 cells per well, for time-lapse survival assays and 3×10^5 cells per well, for mass spectrometry). All dishes and plates were coated with poly-L-lysine (Sigma-Aldrich) one week before use. Cultures were maintained in neurobasal medium supplemented with B27 (Invitrogen), 0.5 mM L-glutamine, 0.025 mM glutamate at 37 °C in a humidified atmosphere containing 5% CO_2. All experiments were performed on neuronal cultures at 7–11 days *in vitro* (DIV) ensuring that dendritic/axonal structures were established and cells expressed a full complement of CBR proteins.

2.4 Immunocytochemistry

PFC neuronal cultures were fixed in 4% paraformaldehyde for 10 min, and then incubated in blocking buffer (1% normal goat serum, 4% BSA in 1x PBS) for 1 h at room temperature. Neuronal cultures were then incubated with primary antibodies against MAP2ab (mouse, Millipore, MAB378; 1:500), and CB_1R-NH (raised to amino acids 1–77 of the N-terminus; rabbit, 1:500; (Tsou et al., 1998)), or glial fibrillary acidic protein (GFAP; rabbit, Millipore, AB5804; 1:500), diluted in blocking buffer, overnight at 4 °C. For detecting neurons that undergo apoptosis, cultures were incubated with antibodies against mouse/human active caspase-3 (rabbit, R&D Systems, AF835-SP, 1:2000) and NeuN (mouse, Millipore, MAB377. 1:100). Primary antibodies were detected using appropriate secondary antibodies conjugated to either goat-anti-mouse Alexa 488 (Molecular Probes, O-6380, 1:1000) or goat-anti-rabbit Alexa 594 (Molecular Probes, A11012; 1:500). Secondary antibodies were diluted in blocking buffer and applied to the coverslips for 1 h at room temperature. Neurons were then washed thoroughly with 1x PBS, counterstained with Hoechst 33342 for 3 min and mounted using ProLong Gold (Molecular Probes, P36930). Immunofluorescent images were acquired using either a Zeiss LSM 700 laser scanning confocal microscope equipped with a 63x oil immersion objective (Zeiss, Thornwood, NY) or Zeiss Axio Observer Z.1 inverted microscope equipped with a 40x oil immersion objective. The percent astrocytes composition of neuronal cultures was calculated by dividing the number of GFAP-positive cells by the total number of MAP2ab- and GFAP-positive cells visualized from 10–20 randomly collected images. At least three independent experiments were run for each treatment group per time point (DIV 7 & DIV 11). It should be noted that microglial cells that stained positive for Iba1 are a negligible component of our PFC neuronal cultures making up less than 0.1% of observed cells (data not shown). Z-stacks for Imaris analysis were collected using ZEN 2010 blue Edition software (Zeiss, Inc.) and single images were

generated using the orthogonal projection function. Adobe Photoshop CS6 Extended 13.0 software (Adobe Systems, Inc.; San Jose, CA) was used to edit the images.

2.5 Calcium imaging

Live cell imaging was conducted on living PFC neurons in culture using a Zeiss Axio Observer Z.1 inverted microscope (20x objective) with an automated, computer-controlled stage encoder with environmental control (37°C, 95% humidity, 5% CO_2). The cell permeant acetoxymethyl (AM) ester-linked $[Ca^{2+}]_i$ indicator fura-2AM (Kd = 145 nM; 2.5 μM, Molecular Probes) was used for measuring $[Ca^{2+}]_i$ and diluted in Hank's balanced salt solution (HBSS with Ca^{2+}, Invitrogen) with HEPES (10 mM, Invitrogen) according to manufacturer's instructions. Neurons were imaged for a 30 min period. Using ZEN 2010 blue Edition software, images were acquired with a MRm digital camera (Zeiss) at a frame rate of 0.2 Hz during the first 5 min, 0.033 Hz from 5 min to 10 min, and 0.0166 Hz from 10 to 30 min. Relative fluorescence ratio images were acquired at 340/380 nm excitation and 510 nm emission wavelengths. Conversion to $[Ca^{2+}]_i$ was calculated according to an equation described previously (Grynkiewicz G Fau - Poenie et al., 1985). Regions of interest (ROIs) were manually assigned to neuronal somata. Due to the heterogeneity among neurons, the mean ± SEM values for changes in $[Ca^{2+}]_i$ were computed comparing individual neurons before and at specific intervals during treatment using a repeated-measure analysis of variance (ANOVA). Quantitative analyses of $[Ca^{2+}]_i$ levels in neuronal somata were performed on 12–15 randomly selected neurons per treatment per experiment. At least three independent experiments were run for each treatment group.

2.6 Dendrite morphology and Imaris reconstruction

To assess changes in dendritic length (μm), dendritic volume ($μm^3$), and number of process filaments of neurons, PFC cultures were exposed to Tat 100 nM for 24 h before being fixed and stained against MAP2ab (see above). 20–30 neurons were imaged per condition using the Zeiss LSM 700 confocal microscope. Z-stacks were reconstructed as 3D images using Imaris software (South Windsor, CT). Dendrites were drawn using the autoloop function starting at the cell surface and ending at the terminus of each process. Dendrite volume was determined using the built-in dendrite volume reconstruction algorithm. All process length, volume, and filament values were calculated by Imaris and exported for statistical analysis. At least three independent experiments were run for each treatment group.

2.7 Neuronal survival

PFC neuronal survival was assessed over a 72 h time period using a Zeiss Axio Observer Z.1 inverted microscope with an automated, computer-controlled stage encoder with environmental control (37 °C, 95% humidity, 5% CO2). Time-lapse studies were conducted as previously described (Zou et al., 2011; Xu et al., 2017). PFC neurons were grown in 12-well plates and 6 non-overlapping fields were selected per well. Individual neurons were then randomly selected from each field and changes in their morphology were assessed over time. Time-lapse images were recorded at 1 h intervals for 72 h using an automated, computer-controlled stage encoder running Zen 2011 software (Zeiss, Inc.). Neuronal death was assessed using rigorous morphological criteria, including neurite disintegration, loss of

phase brightness and fragmentation of the cell body. At least three independent experiments were run for each treatment.

To verify the extent of cell death assessed by the time-lapse survival studies, activated caspase-3 staining was used to detect apoptotic cells in our PFC cultures. Neurons stained with anti-NeuN and anti-activated caspase-3 were imaged using the Zeiss Axio Observer Z.1 microscope, and the number of activated caspase-3 positive neurons was compared to the total number of NeuN positive neurons to determine the percentage of neurons undergoing apoptotic cell death. 10–15 images were randomly collected for each experimental condition from three independent experiments. Results are shown as the fold increase of caspase-3 positive neurons in each condition (DIV 11) compared to the control baseline condition (DIV 8).

2.8 Lipid extraction and mass spectrometry analysis

Cells were dissociated and centrifuged at $5000g$ for 10 min at 4 °C. Cells were stored at −80 °C until analysis. A seven point calibration curves ranged from 0.028 pmol to 2.8 pmol for anandamide (AEA), 0.033 pmol to 3.3 pmol for palmitoylethanolamide (PEA), and 0.031 pmol to 3.1 pmol for oleoylethanolamine (OEA). A negative control and blank control were prepared for each condition. ISTDs (10 μL of ethanol containing of each the following 0.28 pmol AEA-d_8, 0.33 pmol PEA-d_4, and 0.31 pmol OEA-d_4) was added to each calibrator, control, and sample except the blank control. Samples were then homogenized in 100 μL of ethanol and then 900 μL of water was added. Each calibrator, control, and sample was then extracted using a UCT Clean Up® C18 sold phase extraction column (UCT, Inc., Bristol, PA). The columns were conditioned with 3 mL of methanol followed by 3 mL of deionized water. The samples were added to the columns and aspirated followed by 2 mL of deionized water. Lipids were then eluted with 2 mL of methanol. The extracts were evaporated under nitrogen and reconstituted in 50 μL of mobile phase and placed in auto-sampler vial for Ultrahigh Performance Liquid Chromatography (UPLC) tandem mass spectrometry (MS/MS) analysis. UPLC-MS/MS analysis of AEA, PEA, and OEA was performed on a Sciex 6500 QTRAP system with an IonDrive Turbo V source for TurboIonSpray® (Sciex, Ontario, Canada) attached to a Shimadzu UPLC system (Kyoto, Japan) controlled by Analyst software (Sciex, Ontario, Canada). Chromatographic separation of AEA, PEA, and OEA was performed on a Discovery® HS C18 Column 15 cm x 2.1mm, 3 μm (Supelco: Bellefonte, PA) kept at 25°C. The mobile phase consisted of A: acetonitrile and B: water with 1 g/L ammonium acetate and 0.1% formic acid. The following gradient was used: 0.0 to 2.4 min at 40% A, 2.5 to 6.0 min at 40% A, hold for 2.1 min at 40% A, then 8.1 to 9 min 100% A, hold at 100% A for 3.1 min and return to 40% A at 12.1 min with a flow rate was 1.0 mL/min. The source temperature was set at 600°C and had a curtain gas at a flow rate of 30 ml/min. The ionspray voltage was 5000 V with ion source gases 1 and 2 flow rates of 60 and 50 ml/min, respectively. The mass spectrometer was run in positive ionization mode for AEA, PEA and OEA. The acquisition mode used was multiple reaction monitoring (MRM). The following transition ions (m/z) with their corresponding collection energies (eV) in parentheses were used: AEA: 348>62 (13) and 348>91 (60); AEA-d_8: 356>63 (13); PEA: 300>62 (28) and 300>283 (19); PEA-d_4: 304>62 (28); OEA: 326>62 (30) and 326>309 (20); OEA-d_4: 330>66 (30). The total run time for the

analytical method was 14 min. Calibration curves were analyzed with each analytical batch for each analyte. A linear regression of the ratio of the peak area counts of analyte and the corresponding deuterated ISTDs versus concentration was used to construct the calibration curves. Final AEA, PEA and OEA concentrations were normalized by cell collection numbers. At least three independent experiments were run for each treatment.

2.9 Statistical Analyses

Data were analyzed using analyses of variances (ANOVAs) with Bonferroni's correction as necessary (SPSS Statistics, Version 24, IBM). For experiments that included various control groups (pretreatment alone groups, including PF3548, SR1, AM630) only the actual "control" (no drug) group was integrated in statistical analysis as no significant differences were noted between any of the control groups. Violations of compound symmetry in repeated-measures ANOVAs for the within-subjects factors (i.e., comparing time points) were addressed by using the Greenhouse-Geisser degrees of freedom correction factor (Greenhouse and Geisser, 1959). An alpha level of $p < 0.05$ was considered significant for all statistical tests. Statistics not shown in the text were found to be non-significant. Data are expressed as the mean ± standard error of the mean (SEM). Investigators were blind to the identity of all experimental conditions during analysis.

3.   Results

3.1   Immunocytochemistry

Cell cultures were imaged to visualize cell types and determine the presence of CB_1R (Figure 1). Differentiated neurons (DIV 7–11) were treated with antibodies specific to MAP2ab (green), CB_1R-NH (red) and counterstained with Hoechst 33342 (blue; Figure 1A). Neurons stained positive for MAP2ab and show CB_1R expression localized in the neuronal somata and dendritic processes. No positive CB_1R staining was detected in tissue derived from CB_1R knockout mice (data not shown). Immunocytochemistry indicates that CB_1R is present in PFC neuronal cultures and thus may be sensitive to increases in endocannabinoid signaling following FAAH enzyme inhibition using PF3845. Using a primary antibody specific to GFAP (red) glial cells can be detected alongside neurons (MAP2ab, green; Figure 1B). Quantification of percent astrocytes were taken from neuronal cultures at DIV 7 and DIV 11 respective to when calcium experiments were conducted, and when neuronal survival experiments ended. A small but significant percentage of glia was noted in the cell population of our neuronal cultures (10.8 ± 0.86; $t(65) = 12.5$, $p < 0.001$; Figure 1B'). A two-way ANOVA did not reveal any significant main effects for time [$F(1, 61) = 3.44$, $p = 0.068$], treatment [$F(1, 61) = 2.26$, $p = 0.138$], or time x treatment interaction [$F(1, 61) = 0.34$, $p = 0.560$], indicating that the percent ratio of glia to neurons did not significantly change over the entirety of the experimental time course. When evaluating each cell population independently, a two-way ANOVA showed a significant reduction in neuronal and astroglial populations over time (72 h), indicated by a significant main effect for time for both GFAP+ astrocytes [$F(1, 61) = 6.43$, $p = 0.014$; Figure 1B''] and MAP2ab+ neurons [$F(1, 61) = 138.68$, $p < 0.001$; Figure 1B''']. There was also a significant time x treatment interaction for neurons [$F(1, 61) = 6.17$, $p = 0.016$; Figure 1B'''], suggesting that Tat treatment further decreases neuron count over the 72 h time period.

3.2 Calcium imaging

$[Ca^{2+}]_i$ levels were assessed over time in PFC neuronal cultures to evaluate the potential neuroprotective effects of PF3845 after Tat exposure (Figure 2).

3.2.1 Tat increases $[Ca^{2+}]_i$ levels in PFC cultured neurons in a concentration dependent manner.

—Neurons were incubated with fura-2AM to visualize live changes in $[Ca^{2+}]_i$ over a 30 min period (Figure 2A). Application of Tat onto cultured PFC neurons induced significant changes in $[Ca^{2+}]_i$ in a concentration dependent manner (Figure 2B). A two-way ANOVA showed a significant main effect for both, time $[F(35, 10255) = 13.2, p_{GG} < 0.001]$ and treatment $[F(5, 293) = 55.8, p < 0.001]$, and a significant treatment x time interaction effect $[F(175, 10255) = 7.0, p_{GG} < 0.001]$. A one-way ANOVA was conducted on the initial time period where $[Ca^{2+}]_i$ increase (1–5 min), and during the latter time period (20–30 min) where $[Ca^{2+}]_i$ decreases slightly and plateaus. A significant treatment effect was noted for the initial $(F(5, 293) = 38.3, p < 0.001)$ and the latter neuronal response $(F(5, 293) = 33.3, p < 0.001)$. During the initial phase, Tat 100 nM and 500 nM conditions significantly increased $[Ca^{2+}]_i$ levels compared to control, Tat 5 nM, 10 nM, and 50 nM conditions $(p < 0.001)$. The Tat 500 nM effect on $[Ca^{2+}]_i$ levels was also significantly greater compared to the Tat 100 nM treatment effect $(p = 0.003)$. For the latter phase the same group differences were found as reported for the initial phase.

3.2.2 PF3845 blunts Tat-mediated increases in neuronal $[Ca^{2+}]_i$ levels in a concentration dependent manner.

—Pretreating cultured PFC neurons with PF3845 blunts Tat 100 nM-mediated increases in $[Ca^{2+}]_i$ levels in a concentration dependent manner (Figure 2C). A two-way ANOVA revealed a significant main effect of time $[F(35, 9625) = 11.2, p_{GG} < 0.001]$ and treatment $[F(5, 275) = 14.2, p < 0.001]$, and a significant treatment x time interaction effect $[F(175, 9625) = 2.6, p_{GG} < 0.001]$. A one-way ANOVA conducted on the initial $[Ca^{2+}]_i$ phase demonstrated a significant treatment effect $[F(5, 269) = 19.7, p < 0.001]$ with all concentrations of PF3845 (10, 50, 100 nM) + Tat 100 nM reducing $[Ca^{2+}]_i$ levels compared to the Tat 100 nM condition $(p = 0.046, p = 0.003, p < 0.001;$ respectively). Note that only the PF3845 100 nM + Tat condition was able to maintain $[Ca^{2+}]_i$ levels at values that were not significantly different from control. For the latter phase, a one-way ANOVA also demonstrated a significant treatment effect $[F(5, 268) = 7.8, p < 0.001]$, with the PF3845 100 nM condition resulting in significantly reduced $[Ca^{2+}]_i$ levels compared to the Tat 100 nM only condition $(p = 0.002)$, and showing no significant difference from control.

3.2.3 PF3845 blunting effect on $[Ca^{2+}]_i$ levels is CB_1R, but not CB_2R, dependent.

—Using selective CB_1R and CB_2R antagonists (SR1 and AM630, respectively) it was determined that the specificity of PF3845's neuroprotective effect on Tat-exposed PFC neurons (Figure 2D). A two-way ANOVA revealed a significant main effect for time $[F(35, 8540) = 9.49, p_{GG} < 0.001]$ and treatment $[F(4, 244) = 14.00, p < 0.001]$, and a significant treatment x time interaction effect $[F(140, 8540) = 2.84, p_{GG} < 0.001]$. A one-way ANOVA conducted on the initial $[Ca^{2+}]_i$ phase revealed a significant treatment effect $[F(4, 246) = 20.04, p < 0.001]$, with SR1 50 nM blocking the protective effect of PF3845 against Tat-induced increase in $[Ca^{2+}]_i$ levels (SR1 50 nM + PF3845 100 nM + Tat 100 nM;

$p < 0.001$ vs. control; $p = 0.040$ vs. AM630 50 nM + PF3845 100 nM + Tat 100 nM). In contrast, the CB$_2$R antagonist AM630 50 nM revealed no significant difference from control in combination with PF3845 100 nM + Tat 100 nM and showed significant lower [Ca^{2+}]$_i$ levels from Tat 100 nM ($p < 0.001$), thus failing to prevent the protective effects of PF3845 100 nM against Tat-induced [Ca^{2+}]$_i$ level increases. In the latter phase the one-way ANOVA indicated a significant treatment effect [$F_{(4, 246)} = 7.65$, $p < 0.001$] with similar group differences as reported for the initial phase. None of the various control conditions, including PF3845 100 nM, SR1 50 nM, and AM630 50 nM, varied significantly from the control group across any of the presented phases.

3.3 Morphological changes quantified by Imaris analysis

Considering synapto-dendritic injury plays an essential role in the pathogenesis of HAND we examined Tat and FAAH enzyme inhibitor PF3845 effects after 24 h on dendritic morphology (length, volume, process filaments) using Imaris for quantification (Figure 3). Neurons were visualized as 3D representations and individual dendritic processes were analyzed (Figure 3A). A one-way ANOVA on total dendritic length (µm) showed a significant treatment effect [$F_{(4, 82)} = 10.13$, $p < 0.001$], with a significant decrease of dendritic length by all Tat treatment conditions (Figure 3B). A one-way ANOVA on total dendritic volume (µm^3) revealed a significant treatment effect [$F_{(4, 82)} = 18.96$, $p < 0.001$] with a significant downregulation of dendritic volume by Tat 100 nM ($p < 0.001$, Figure 3C). Importantly, pretreating Tat-exposed neurons with PF3845 100 nM significantly increased volume of dendrites, indicating a protective effect of PF3845 against Tat-induced downregulation of dendritic volume ($p < 0.001$). Interestingly, pretreating PF3845 100 nM + Tat 100 nM-exposed neurons with AM630 but not SR1 blocked the protective effects of PF3845 100 nM against Tat toxicity, implying an underlying CB$_2$R-related mechanism for synapto-dendritic injury after 24 h Tat treatment, specifically when looking at total dendritic volume. Lastly, a one-way ANOVA on the total number of dendritic filaments revealed no significant treatment effect [$F_{(4, 88)} = 0.48$, $p = 0.748$], indicating that the dendritic filament number did not change significantly for any treatment condition (Figure 3D). None of the various control conditions, including PF3845 100 nM, SR1 50 nM, and AM630 50 nM, varied significantly from the control group.

3.4 Neuronal survival

Neuronal survival after PF3845 ± Tat exposure over a 72 h time period was assessed to evaluate the potential protective effects of PF3845 against neuronal death (Figure 4).

3.4.1 Tat potentiates neuronal death in a concentration dependent manner.—

Neurons were visualized using phase-contrast microscopy (Figure 4A). Challenging neurons with Tat for 72 h decreased neuronal viability in a Tat dose dependent fashion (Figure 4B). A two-way ANOVA on neuronal survival demonstrated a significant main effect of time [$F_{(18, 1224)} = 140.8$, $p_{GG} < 0.001$] and a significant treatment x time interaction [$F_{(54, 1224)} = 3.4$, $p_{GG} < 0.001$]. A one-way ANOVA conducted on the last 72nd h time point indicated a significant treatment effect [$F_{(3, 68)} = 4.0$, $p = 0.011$], with Tat 100 nM condition significantly reducing neuronal survival compared to control ($p < 0.016$).

3.4.2 PF3845 increases neuronal survival after Tat exposure in a concentration dependent manner.—Pretreating neurons with different concentrations of PF3845 produce neuroprotective effects against Tat-exposure (Figure 4C). For the two-way ANOVA a significant effect was noted for time [$F(18, 1224) = 153.3$, $p_{GG} < 0.001$] and treatment x time interaction [$F(54, 1224) = 4.2$, $p_{GG} < 0.001$]. A one-way ANOVA on the 72nd h time point revealed a significant treatment effect [$F(3, 68) = 4.0$, $p = 0.012$], with Tat 100 nM and PF3845 50 nM + Tat significantly reducing neuronal survival compared to control ($p = 0.039$ and $p = 0.033$, respectively). In contrast, the higher PF3945 100 nM concentration protected against neuronal death, with PF3845 100 nM + Tat showing no significant difference from control.

3.4.3 PF3845 protective effects on neuronal death are CB$_2$R dependent.—
Using selective CB$_1$R and CB$_2$R antagonists (SR1 and AM630, respectively) it was determined which of these receptors mediated PF3845's neuroprotective effect against Tat-mediated neuronal death (Figure 4D). A two-way ANOVA showed a significant effect for time [$F(18, 3366) = 338.40$, $p_{GG} < 0.001$] and treatment x time interaction [$F(72, 3366) = 4.73$, $p_{GG} < 0.001$]. A one-way ANOVA on the 72nd h time point revealed a significant treatment effect [$F(4, 187) = 6.32$, $p < 0.001$], with Tat and Tat + AM630 significantly reducing neuronal survival from control. None of the various control conditions, including PF3845 100 nM, SR1 50 nM, and AM630 50 nM, significantly affected cell death compared to the control group.

3.4.4 PF3845 decreases activated caspase-3 positive neurons following Tat exposure.—Using antibodies against activated caspase-3 and NeuN, it was possible to quantify the number of neurons expressing activated caspase-3 after 72 h of Tat exposure (Figure 4F). A one-way ANOVA demonstrated a significant main effect for treatment [$F(4, 45) = 10.79$, $p < 0.001$] with Tat 100 nM and AM630 + PF + Tat significantly increasing the number of caspase-3 positive neurons. This provides further evidence that PF3845 protects against Tat-mediated apoptotic cell death via a CB$_2$R-dependent mechanism. None of the various control conditions, including PF3845 100 nM, SR1 50 nM, and AM630 50 nM, varied significantly from the control group.

3.5 Mass spectrometry

UPLC-MS/MS was used to determine the expression of AEA and other predominant substrates of FAAH in the presence of PF3845 100 nM ± Tat 100 nM (Figure 5). Neurons exposed to PF3845 ± Tat were collected after 30 min for analysis of AEA, PEA, and OEA concentrations. 2-AG levels were not assessed as past literature demonstrated that PF3845 administration does not significantly alter 2-AG concentration in brain tissue (Ahn et al., 2009; Booker et al., 2012). A two-way ANOVA found a significant main effect of PF3845 for both AEA [$F(1,12) = 6.16$, $p = 0.029$] and PEA [$F(1,11) = 6.77$, $p = 0.025$], but not OEA [$F(1,12) = 2.11$, $p = 0.172$]. No significant main effect for Tat treatment was found for either AEA [$F(1,12) = 1.26$, $p = 0.284$], PEA [$F(1,11) = 1.91$, $p = 0.195$], or OEA [$F(1,12) = 0.11$, $p = 0.748$]. Additionally no significant PF3845 x Tat interactions were noted, AEA [$F(1,12) = 0.03$, $p = 0.861$], PEA [$F(1,11) = 0.60$, $p = 0.455$], and OEA [$F(1,12) = 3.14$, $p = 0.102$]. As hypothesized, PF3845 100 nM significantly increased concentrations of some lipids targeted

by FAAH, represented by an approximate 2-fold increase in AEA concentration and an approximate 5-fold increase in PEA concentration in the control vs. PF3845 ± Tat conditions. No significant effect main effect was found for any OEA condition.

4.1 Discussion

Our results demonstrate that a highly selective FAAH inhibitor, PF3845, inhibits increases in neuronal $[Ca^{2+}]_i$ levels, promotes cell survival, and prevents loss of normal dendrite morphology in Tat treated murine PFC neuronal cultures. These effects were mediated via a CB_1R and/or CB_2R and likely induced by increased endocannabinoid signaling following FAAH inhibition. The $[Ca^{2+}]_i$ imaging results show that neurons exposed to Tat 100 nM significantly increase intracellular calcium in a stereotypical fashion (initial and latter phases of $[Ca^{2+}]_i$ increase) similar to what has been described earlier (Brailoiu et al., 2008b). This increase in calcium is a combination of Ca^{2+} influx as a consequence of NMDA receptor activation (Haughey et al., 2001; Perez et al., 2001; Longordo et al., 2006; Fitting et al., 2014) and release of Ca^{2+} from intracellular stores mediated via inositol 1,4,5-trisphosphate (IP_3) and/or ryanodine receptor pathways (Haughey et al., 1999; Fitting et al., 2014). The Tat-mediated $[Ca^{2+}]_i$ effect shows differential sensitivity to various concentrations of PF3845. While PF3845 100 nM significantly blunts $[Ca^{2+}]_i$ levels across the entire time period, lower concentrations (i.e. 10 nM and 50 nM) only significantly blunt the initial phase of the Tat effect. Considering that the initial spike in Tatmediated $[Ca^{2+}]_i$ primarily results from Ca^{2+} release from intracellular stores (Chami et al., 2006), the presented data suggest that Tat's influence on IP_3/ryanodine receptor pathways is more sensitive to PF3845 treatment than NMDAR activity. The role of CB_1R in protecting neurons from NMDA-induced cytotoxicity has been shown to be IP_3 receptor dependent (Liu et al., 2009), and intracellular CB_1R activity has been linked with accessing lysosome and endoplasmic reticulum calcium stores (Brailoiu et al., 2011) suggesting that CB_1R activation may disrupt the ability of Tat to exert its effects on $[Ca^{2+}]_i$. CB_1R has also been found to form heterodimers with NMDARs (Sanchez-Blazquez et al., 2014) and disrupting the formation of this complex has been shown to block the ability of CB_1R to attenuate damage from excitotoxic insults (Vicente-Sanchez et al., 2013).

When examining the neurotoxic effects of Tat it is also important to consider the role of disruptions in healthy dopamine signaling. A potential alternative/complementary explanation for the effects that we have observed stems from Tat's ability to bind and inhibit dopamine transporter activity (DAT) (Quizon et al., 2016) leading to increased dopamine levels which could contribute to neurotoxic conditions. Interestingly, human DAT activity in HIV-1 patients negatively correlates with HAND symptom severity (Wang et al., 2004; Chang et al., 2008) suggesting it plays an important role in the development of HAND pathology. While outside the scope of the experiments presented here, exploring the effect of Tat on the dopaminergic system and how it interacts with cannabinoid signaling in our culture model could offer additional insights into developing effective treatments for HAND patients.

While CB_1R activity played a significant role in reducing Tat-mediated neurotoxicity, CB_2R activity also played an essential role in neuronal survival and protecting against Tat-induced

decreases in dendritic volume. Using SR1 and AM630 showed that PF3845 ameliorated Tat mediated neuronal death and loss of dendritic structure through CB_2R signaling, but independently of CB_1R signaling. This finding suggests that the 11% astroglial component of our cultures (Figure 1B') likely plays a role in these protective effects, as glia such as murine astrocytes are known to express CB_2R (Stella, 2010) and contribute to ion buffering, regulation of neurotransmitters, and supporting neuronal growth (Newman, 2003; Lian and Stringer, 2004; Rossi, 2015). A similarly small population of glia have been observed in earlier reports using this culture model (Fitting et al., 2014). Morphine was shown to potentiate Tat-mediated neurotoxicity via μ-opioid receptors in striatal neuronal cultures but based on earlier findings these effects were found to be astrocyte specific (Zou et al., 2011), suggesting that even a small population of glial cells can play a significant role in attenuating Tat-mediated neurotoxicity. Glial cells expressing CB_2R's been demonstrated to be viable targets for protecting neurons from HIV-1 associated neurodegeneration as shown in several models of HAND (Price et al., 2009; Kim et al., 2011; Hu et al., 2013), which indicates the importance of targeting neuroinflammatory signaling in this condition. Alternatively, evidence exists that suggests that CB_2R is sparsely expressed in neuronal populations, some which have been found in the ventral tegmental area (VTA) and hippocampus (Zhang et al., 2016; Li and Kim, 2017). Therefore, it would be necessary for further study to detect the presence or lack thereof CB_2R in murine PFC and ascertain its potential role in influencing Tat-mediated neuronal damage.

Disruption of synaptic structures is a major component of HAND and the prevention and/or reversibility of this damage is of major interest to the field (Ellis et al., 2007). In the present study neurons were exposed to PF3845 ± Tat and reconstructed to characterize the changes in neuronal dendritic morphology. Decreases in MAP2ab staining in human frontal cortex has been associated with higher viral load and decreased neurocognitive function in HIV-1 infected individuals (Levine et al., 2016), and direct treatment of cultured hippocampal neurons with Tat has been shown to decrease MAP2ab expression (Butler et al., 2011). The analysis of the results revealed an interesting interaction between Tat and PF3845 where PF3845 failed to effect Tat-mediated loss of dendritic length but did preserve overall dendritic volume. Because there was not a significant alteration in the total number of process filaments per neuron in each condition this suggests that PF3845 increases the cross-sectional area of the MAP2ab expressed within the individual dendritic structures. This could be indicative of dendritic swelling, which has been reported to result from Tat infliction (Xu et al., 2017), and is known to precede further degeneration in multiple models of neurodegenerative conditions (Jaworski et al., 2011; Chen et al., 2017). The differences between the Tat and PF3845 + Tat conditions suggests that PF3845 treatment may slow or halt the progression of synaptodendritic damage mediated by Tat. Our lab has shown that Tat attenuates GABAergic function in our current culture model, which can be blocked by application of CB_1R agonists (Xu et al., 2016). This demonstrates that while our cultures are relatively immature at DIV 7, functional consequences of Tat infliction can be quantified. In the future we plan to use older cultures to allow for further observation of functional changes in neuronal morphology (e.g. dendritic spine morphology/density) and the resulting data will be essential in ascertaining PF3845's ability in preserving neuronal functionality and/or reversing damage following Tat infliction.

The neuroprotective effects of PF3845 in our Tat-exposed PFC neuronal cultures may be due to the elevation of AEA and/or PEA concentrations. Increases in PEA alongside AEA were of great interest because this fatty acid amide has been shown to produce anti-inflammatory and neuroprotective activity through the peroxisome proliferator-activated receptor family (Landreth, 2007; Bright et al., 2008; Scuderi et al., 2012; Paterniti et al., 2014). A previous study using murine brain tissue demonstrated increased expression of endogenous N-acylethanolamide molecules, including AEA and PEA following administration of PF3845 (Wiebelhaus et al., 2015).

Overall these findings indicate that inhibiting FAAH activity can protect neurons against Tat infliction. This raises the question if the removal of HIV-1 related stressors on neurons may elicit dendritic regeneration and restoration of cognitive function. Therefore, while PF3845 was effective in attenuating Tat-mediated neurotoxicity, it will be important to further explore whether its application can reverse pre-existing Tat-induced neuronal injuries.

5.1 Conclusion

The presented data show the capacity of the HIV-1 Tat protein to destabilize neuronal calcium equilibrium, increase neuronal death, and mediate dendritic degeneration while application of the highly selective and potent FAAH inhibitor, PF3845, is able to attenuate these effects. The results of the calcium experiments supported the hypothesis that enhancing AEA concentration using PF3845 will produce neuroprotective effects via neuronal CB_1R. The findings that the CB_2R played a key role in attenuating Tat mediated increases in neuronal death and dendritic degeneration over 72 and 24 h, respectively, suggest that CB_2Rs likely play a pertinent role in Tat-mediated neurodegeneration and can be targeted for therapeutic benefit by drugs such as PF3845. In addition, it will be important to evaluate the potential role of specific CB_2R ligands as therapeutic drugs in treatment of HAND. Future experiments will be necessary to further understand the interaction between Tat and CNS resident neurons and glial cells in the pathogenesis of HAND and how pharmaceutical agents targeting the endogenous cannabinoid system can potentially block or reverse these neurodegenerative conditions.

Acknowledgements

Abbreviations

2-AG	2-arachidonoylglycerol
Anandamide/AEA	N-arachidonoylethanolamine
CB1R	cannabinoid type 1 receptor
CB2R	cannabinoid type 2 receptor
cART	combined antiretroviral therapy

DAT	dopamine transporter
DIV	days *in vitro*
FAAH	fatty acid amide hydrolase
HIV-1	human immunodeficiency virus 1
HAND	HIV-1 associated neurocognitive disorders
ISTD	internal standard
MAGL	monoacylglycerol lipase
MS/MS	tandem mass spectrometry
neuroAIDS	neuro-acquired immune deficiency syndrome
OEA	oleoylethanolamine
PEA	palmitoylethanolamide
PFC	prefrontal cortex
SR1	SR141716a
Tat	transactivator of transcription
UPLC	ultrahigh performance liquid chromatography

References

Ahn K, Johnson DS, Mileni M, Beidler D, Long JZ, McKinney MK, Weerapana E, Sadagopan N, Liimatta M, Smith SE, Lazerwith S, Stiff C, Kamteka S., Bhattacharya K., Zhang Y., Swaney S., Van Becelaere K., Stevens RC., Cravatt BF., 2009 Discovery and characterization of a highly selective FAAH inhibitor that reduces inflammatory pain. Chemistry & biology 16, 411–420. [PubMed: 19389627]

Behnisch T, Francesconi W, Sanna PP, 2004 HIV secreted protein Tat prevents long-term potentiation in the hippocampal CA1 region. Brain Res 1012, 187–189. [PubMed: 15158177]

Bertrand SJ, Mactutus CF, Aksenova MV, Espensen-Sturges TD, Booze RM, 2014 Synaptodendritic recovery following HIV Tat exposure: neurorestoration by phytoestrogens. J Neurochem 128, 140–151. [PubMed: 23875777]

Bonavia R, Bajetto A, Barbero S, Albini A, Noonan DM, Schettini G, 2001 HIV-1 Tat causes apoptotic death and calcium homeostasis alterations in rat neurons. Biochem Biophys Res Commun 288, 301–308. [PubMed: 11606043]

Booker L, Kinsey SG, Abdullah RA, Blankman JL, Long JZ, Ezzili C, Boger DL, Cravatt BF, Lichtman AH, 2012 The fatty acid amide hydrolase (FAAH) inhibitor PF-3845 acts in the nervous system to reverse LPS-induced tactile allodynia in mice. Br J Pharmacol 165, 2485–2496. [PubMed: 21506952]

Brailoiu GC, Brailoiu E, Chang JK, Dun NJ, 2008a Excitatory effects of human immunodeficiency virus 1 Tat on cultured rat cerebral cortical neurons. Neuroscience 151, 701–710. [PubMed: 18164555]

Brailoiu GC, Brailoiu E, Chang JK, Dun NJ, 2008b Excitatory effects of human immunodeficiency virus 1 Tat on cultured rat cerebral cortical neurons. Neuroscience 151, 701–710. [PubMed: 18164555]

Brailoiu GC, Oprea TI, Zhao P, Abood ME, Brailoiu E, 2011 Intracellular cannabinoid type 1 (CB1) receptors are activated by anandamide. J Biol Chem 286, 29166–29174. [PubMed: 21719698]

Bright JJ, Kanakasabai S, Chearwae W, Chakraborty S, 2008 PPAR Regulation of Inflammatory Signaling in CNS Diseases. PPAR Res 2008, 658520. [PubMed: 18670616]

Butler TR., Smith KJ., Self RL., Braden BB., Prendergast MA., 2011 Neurodegenerative effects of recombinant HIV-1 Tat(1–86) are associated with inhibition of microtubule formation and oxidative stress-related reductions in microtubule-associated protein-2(a,b). Neurochem Res 36, 819–828. [PubMed: 21259049]

Carroll A, Brew B, 2017 HIV-associated neurocognitive disorders: recent advances in pathogenesis, biomarkers, and treatment. F1000Res 6, 312. [PubMed: 28413625]

Chami M, Oules B, Paterlini-Brechot P, 2006 Cytobiological consequences of calcium-signaling alterations induced by human viral proteins. Biochim Biophys Acta 1763, 1344–1362. [PubMed: 17059849]

Chang L, Wang GJ, Volkow ND, Ernst T, Telang F, Logan J, Fowler JS, 2008 Decreased brain dopamine transporters are related to cognitive deficits in HIV patients with or without cocaine abuse. Neuroimage 42, 869–878. [PubMed: 18579413]

Chen X, Jiang XM, Zhao LJ, Sun LL, Yan ML, Tian Y, Zhang S, Duan MJ, Zhao HM, Li WR, Hao YY, Wang LB, Xiong QJ, Ai J, 2017 MicroRNA-195 prevents dendritic degeneration and neuron death in rats following chronic brain hypoperfusion. Cell Death Dis 8, e2850. [PubMed: 28569780]

Cheng J, Nath A, Knudsen B, Hochman S, Geiger JD, Ma M, Magnuson DS, 1998 Neuronal excitatory properties of human immunodeficiency virus type 1 Tat protein. Neuroscience 82, 97–106. [PubMed: 9483506]

Chevaleyre V, Takahashi KA, Castillo PE, 2006 ENDOCANNABINOID-MEDIATED SYNAPTIC PLASTICITY IN THE CNS. Annual Review of Neuroscience 29, 37–76.

Chiarlone A, Bellocchio L, Blazquez C, Resel E, Soria-Gomez E, Cannich A, Ferrero JJ, Sagredo O, Benito C, Romero J, Sanchez-Prieto J, Lutz B, Fernandez-Ruiz J, Galve-Roperh I, Guzman M, 2014 A restricted population of CB1 cannabinoid receptors with neuroprotective activity. Proc Natl Acad Sci U S A 111, 8257–8262. [PubMed: 24843137]

Derkinderen P, Valjent E, Toutant M, Corvol JC, Enslen H, Ledent C, Trzaskos J, Caboche J, Girault JA, 2003 Regulation of extracellular signal-regulated kinase by cannabinoids in hippocampus. J Neurosci 23, 2371–2382. [PubMed: 12657697]

Di Marzo V, 2008 Targeting the endocannabinoid system: to enhance or reduce? Nature Reviews Drug Discovery 7, 438. [PubMed: 18446159]

El-Hage N., Bruce-Keller AJ., Yakovleva T., Bazov I., Bakalkin G., Knapp PE., Hauser KF., 2008 Morphine exacerbates HIV-1 Tat-induced cytokine production in astrocytes through convergent effects on [Ca(2+)](i), NF-kappaB trafficking and transcription. PLoS One 3, e4093. [PubMed: 19116667]

El-Hage N, Dever SM, Fitting S, Ahmed T, Hauser KF, 2011 HIV-1 coinfection and morphine coexposure severely dysregulate hepatitis C virus-induced hepatic proinflammatory cytokine release and free radical production: increased pathogenesis coincides with uncoordinated host defenses. J Virol 85, 11601–11614. [PubMed: 21900165]

Ellis R, Langford D, Masliah E, 2007 HIV and antiretroviral therapy in the brain: neuronal injury and repair. Nat Rev Neurosci 8, 33–44. [PubMed: 17180161]

Fitting S, Knapp PE, Zou S, Marks WD, Bowers MS, Akbarali HI, Hauser KF., 2014 Interactive HIV-1 Tat and Morphine-Induced Synaptodendritic Injury Is Triggered through Focal Disruptions in Na+ Influx, Mitochondrial Instability, and Ca2+ Overload. The Journal of Neuroscience 34, 12850–12864. [PubMed: 25232120]

Fitting S, Ngwainmbi J, Kang M, Khan FA, Stevens DL, Dewey WL, Knapp PE, Hauser KF, Akbarali HI, 2015 Sensitization of enteric neurons to morphine by HIV-1 Tat protein. Neurogastroenterol Motil 27, 468–480. [PubMed: 25703354]

Gannon P, Khan MZ, Kolson DL, 2011 Current understanding of HIV-associated neurocognitive disorders pathogenesis. Curr Opin Neurol 24, 275–283. [PubMed: 21467932]

Greenhouse SW, Geisser S, 1959 On methods in the analysis of profile data. Psychometrika 24, 95–112.

Grynkiewicz G Fau - Poenie M, Poenie M Fau - Tsien RY, Tsien RY, 1985 A new generation of Ca2+ indicators with greatly improved fluorescence properties. J Biol Chem.

Hahn YK, Vo P, Fitting S, Block ML, Hauser KF, Knapp PE, 2010 beta-Chemokine production by neural and glial progenitor cells is enhanced by HIV-1 Tat: effects on microglial migration. J Neurochem 114, 97–109. [PubMed: 20403075]

Hampson RE, Miller F, Palchik G, Deadwyler SA, 2011 Cannabinoid receptor activation modifies NMDA receptor mediated release of intracellular calcium: implications for endocannabinoid control of hippocampal neural plasticity. Neuropharmacology 60, 944–952. [PubMed: 21288475]

Harezlak J, Buchthal S, Taylor M, Schifitto G, Zhong J, Daar E, Alger J, Singer E, Campbell T, Yiannoutsos C, Cohen R, Navia B, Consortium, H. I. V. N., 2011 Persistence of HIV-associated cognitive impairment, inflammation, and neuronal injury in era of highly active antiretroviral treatment. AIDS 25, 625–633. [PubMed: 21297425]

Haughey NJ., Holden CP., Nath A., Geiger JD., 1999 Involvement of inositol 1,4,5-trisphosphate-regulated stores of intracellular calcium in calcium dysregulation and neuron cell death caused by HIV-1 protein tat. J Neurochem 73, 1363–1374. [PubMed: 10501179]

Haughey NJ, Nath A, Mattson MP, Slevin JT, Geiger JD, 2001 HIV-1 Tat through phosphorylation of NMDA receptors potentiates glutamate excitotoxicity. Journal of Neurochemistry 78, 457–467. [PubMed: 11483648]

Heaton RK, Franklin DR, Ellis RJ, McCutchan JA, Letendre SL, LeBlanc S, Corkran SH, Duarte NA, Clifford DB, Woods SP, Collier AC, Marra CM, Morgello S, Mindt MR, Taylor MJ, Marcotte TD, Atkinson JH, Wolfson T, Gelman BB, McArthur JC, Simpson DM, Abramson I, Gamst A, Fennema-Notestine C, Jernigan TL, Wong J, Grant, I., for the, C., Groups, H., 2011 HIV-associated neurocognitive disorders before and during the era of combination antiretroviral therapy: differences in rates, nature, and predictors. Journal of Neurovirology 17, 3–16. [PubMed: 21174240]

Hu S, Sheng WS, Rock RB, 2013 CB2 receptor agonists protect human dopaminergic neurons against damage from HIV-1 gp120. PLoS One 8, e77577. [PubMed: 24147028]

Jaworski T., Lechat B., Demedts D., Gielis L., Devijver H., Borghgraef P., Duimel H., Verheyen F., Kugler S., Van Leuven F., 2011 Dendritic degeneration, neurovascular defects, and inflammation precede neuronal loss in a mouse model for tau-mediated neurodegeneration. Am J Pathol 179, 2001–2015. [PubMed: 21839061]

Jin J, Lam L, Sadic E, Fernandez F, Tan J, Giunta B, 2012 HIV-1 Tat-induced microglial activation and neuronal damage is inhibited via CD45 modulation: A potential new treatment target for HAND. American Journal of Translational Research 4, 302–315. [PubMed: 22937208]

Kim HJ, Shin AH, Thayer SA, 2011 Activation of cannabinoid type 2 receptors inhibits HIV-1 envelope glycoprotein gp120-induced synapse loss. Mol Pharmacol 80, 357–366. [PubMed: 21670103]

King JE, Eugenin EA, Buckner CM, Berman JW, 2006 HIV tat and neurotoxicity. Microbes Infect 8, 1347–1357. [PubMed: 16697675]

Kruman II, Nath A, Mattson MP, 1998 HIV-1 protein Tat induces apoptosis of hippocampal neurons by a mechanism involving caspase activation, calcium overload, and oxidative stress. Exp Neurol 154, 276–288. [PubMed: 9878167]

Landreth G, 2007 Therapeutic use of agonists of the nuclear receptor PPARgamma in Alzheimer's disease. Curr Alzheimer Res 4, 159–164. [PubMed: 17430241]

Levine AJ, Soontornniyomkij V, Achim CL, Masliah E, Gelman BB, Sinsheimer JS, Singer EJ, Moore DJ, 2016 Multilevel analysis of neuropathogenesis of neurocognitive impairment in HIV. Journal of Neurovirology 22, 431–441. [PubMed: 26637429]

Li Q, Yan H, Wilson WA, Swartzwelder HS, 2010 Modulation of NMDA and AMPA-mediated synaptic transmission by CB1 receptors in frontal cortical pyramidal cells. Brain Res 1342, 127–137. [PubMed: 20420813]

Li Y, Kim J, 2017 Distinct roles of neuronal and microglial CB2 cannabinoid receptors in the mouse hippocampus. Neuroscience 363, 11–25. [PubMed: 28888955]

Lian XY, Stringer JL, 2004 Astrocytes contribute to regulation of extracellular calcium and potassium in the rat cerebral cortex during spreading depression. Brain Res 1012, 177–184. [PubMed: 15158175]

Liu Q, Bhat M, Bowen WD, Cheng J, 2009 Signaling pathways from cannabinoid receptor-1 activation to inhibition of N-methyl-D-aspartic acid mediated calcium influx and neurotoxicity in dorsal root ganglion neurons. J Pharmacol Exp Ther 331, 1062–1070. [PubMed: 19752241]

Longordo F., Feligioni M., Chiaramonte G., Sbaffi PF., Raiteri M., Pittaluga A., 2006 The human immunodeficiency virus-1 protein transactivator of transcription up-regulates N-methyl-D-aspartate receptor function by acting at metabotropic glutamate receptor 1 receptors coexisting on human and rat brain noradrenergic neurones. J Pharmacol Exp Ther 317, 1097–1105. [PubMed: 16489129]

Marsicano G, Goodenough S, Monory K, Hermann H, Eder M, Cannich A, Azad SC, Cascio MG, Gutiérrez SO, van der Stelt M, López-Rodríguez ML, Casanova E, Schütz G, Zieglgänsberger W, Di Marzo V, Behl C, Lutz B, 2003 CB1 Cannabinoid Receptors and On-Demand Defense Against Excitotoxicity. Science 302, 84–88. [PubMed: 14526074]

Masliah E., Heaton RK., Marcotte TD., Ellis RJ., Wiley CA., Mallory M., Achim CL., McCutchan JA., Nelson JA., Atkinson JH., Grant I., 1997 Dendritic injury is a pathological substrate for human immunodeficiency virus-related cognitive disorders. HNRC Group. The HIV Neurobehavioral Research Center. Ann Neurol 42, 963–972. [PubMed: 9403489]

Mattson MP, Haughey NJ, Nath A, 2005 Cell death in HIV dementia. Cell Death Differ 12 Suppl 1, 893–904. [PubMed: 15761472]

Mayne M, Holden CP, Nath A, Geiger JD, 2000 Release of calcium from inositol 1,4,5-trisphosphate receptor-regulated stores by HIV-1 Tat regulates TNF-alpha production in human macrophages. J Immunol 164, 6538–6542. [PubMed: 10843712]

Naidoo V, Nikas S, Karanian D, Hwang J, Zhao J, Wood J, Alapafuja S, Vadivel S, Butler D, Makriyannis A, Bahr B, 2011 A New Generation Fatty Acid Amide Hydrolase Inhibitor Protects Against Kainate-Induced Excitotoxicity. Journal of Molecular Neuroscience 43, 493–502. [PubMed: 21069475]

Nath A, Conant K, Chen P, Scott C, Major EO, 1999 Transient Exposure to HIV-1 Tat Protein Results in Cytokine Production in Macrophages and Astrocytes: A HIT AND RUN PHENOMENON. Journal of Biological Chemistry 274, 17098–17102. [PubMed: 10358063]

Newman EA, 2003 New roles for astrocytes: regulation of synaptic transmission. Trends Neurosci 26, 536–542. [PubMed: 14522146]

Ngwainmbi J, De DD, Smith TH, El-Hage N, Fitting S, Kang M, Dewey WL, Hauser KF, Akbarali HI, 2014 Effects of HIV-1 Tat on enteric neuropathogenesis. J Neurosci 34, 14243–14251. [PubMed: 25339738]

Niphakis MJ, Cognetta AB, 3rd, Chang JW, Buczynski MW, Parsons LH, Byrne F, Burston JJ, Chapman V, Cravatt BF, 2013 Evaluation of NHS carbamates as a potent and selective class of endocannabinoid hydrolase inhibitors. ACS Chem Neurosci 4, 1322–1332. [PubMed: 23731016]

Paterniti I., Cordaro M., Campolo M., Siracusa R., Cornelius C., Navarra M., Cuzzocrea S., Esposito E., 2014 Neuroprotection by association of palmitoylethanolamide with luteolin in experimental Alzheimer's disease models: the control of neuroinflammation. CNS Neurol Disord Drug Targets 13, 1530–1541. [PubMed: 25106636]

Perez A, Probert AW, Wang KK, Sharmeen L, 2001 Evaluation of HIV-1 Tat induced neurotoxicity in rat cortical cell culture. J Neurovirol 7, 1–10.

Perry SW, Barbieri J, Tong N, Polesskaya O, Pudasaini S, Stout A, Lu R, Kiebala M, Maggirwar SB, Gelbard HA, 2010 Human immunodeficiency virus-1 Tat activates calpain proteases via the ryanodine receptor to enhance surface dopamine transporter levels and increase transporter-specific uptake and Vmax. J Neurosci 30, 14153–14164. [PubMed: 20962236]

Pertwee RG, 2014 Elevating endocannabinoid levels: pharmacological strategies and potential therapeutic applications. Proceedings of the Nutrition Society 73, 96–105. [PubMed: 24135210]

Prendergast MA, Rogers DT, Mulholland PJ, Littleton JM, Wilkins LH, Jr., Self RL, Nath A, 2002 Neurotoxic effects of the human immunodeficiency virus type-1 transcription factor Tat require

function of a polyamine sensitive-site on the N-methyl-D-aspartate receptor. Brain Res 954, 300–307. [PubMed: 12414113]

Price DA., Martinez AA., Seillier A., Koek W., Acosta Y., Fernandez E., Strong R., Lutz B., Marsicano G., Roberts JL., Giuffrida A., 2009 WIN55,212–2, a cannabinoid receptor agonist, protects against nigrostriatal cell loss in the 1-methyl-4-phenyl-1,2,3,6-tetrahydropyridine mouse model of Parkinson's disease. Eur J Neurosci 29, 2177–2186. [PubMed: 19490092]

Quizon PM, Sun WL, Yuan Y, Midde NM, Zhan CG, Zhu J, 2016 Molecular mechanism: the human dopamine transporter histidine 547 regulates basal and HIV-1 Tat protein-inhibited dopamine transport. Sci Rep 6, 39048. [PubMed: 27966610]

Rao VR, Ruiz AP, Prasad VR, 2014 Viral and cellular factors underlying neuropathogenesis in HIV associated neurocognitive disorders (HAND). AIDS Res Ther 11, 13. [PubMed: 24894206]

Rappaport J, Joseph J, Croul S, Alexander G, Del Valle L, Amini S, Khalili K, 1999 Molecular pathway involved in HIV-1-induced CNS pathology: role of viral regulatory protein, Tat. J Leukoc Biol 65, 458–465. [PubMed: 10204574]

Rossi D, 2015 Astrocyte physiopathology: At the crossroads of intercellular networking, inflammation and cell death. Prog Neurobiol 130, 86–120. [PubMed: 25930681]

Rossi S, Furlan R, De Chiara V, Muzio L, Musella A, Motta C, Studer V, Cavasinni F, Bernardi G, Martino G, Cravatt BF, Lutz B, Maccarone M, Centonze D, 2011 Cannabinoid CB1 receptors regulate neuronal TNF-alpha effects in experimental autoimmune encephalomyelitis. Brain Behav Immun 25, 1242–1248. [PubMed: 21473912]

Rozzi SJ, Borelli G, Ryan K, Steiner JP, Reglodi D, Mocchetti I, Avdoshina V, 2014 PACAP27 is protective against tat-induced neurotoxicity. Journal of Molecular Neuroscience 54, 485–493. [PubMed: 24696163]

Sacktor N, McDermott MP, Marder K, Schifitto G, Selnes OA, McArthur JC, Stern Y, Albert S, Palumbo D, Kieburtz K, De Marcaida JA, Cohen B, Epstein L, 2002 HIV-associated cognitive impairment before and after the advent of combination therapy. J Neurovirol 8, 136–142. [PubMed: 11935465]

Sanchez-Blazquez P, Rodriguez-Munoz M, Garzon J, 2014 The cannabinoid receptor 1 associates with NMDA receptors to produce glutamatergic hypofunction: implications in psychosis and schizophrenia. Front Pharmacol 4, 169. [PubMed: 24427139]

Scotter EL, Abood Me Fau - Glass M, Glass M, 2010 The endocannabinoid system as a target for the treatment of neurodegenerative disease. Br J Pharmacol.

Scuderi C., Valenza M., Stecca C., Esposito G., Carratu MR., Steardo L., 2012 Palmitoylethanolamide exerts neuroprotective effects in mixed neuroglial cultures and organotypic hippocampal slices via peroxisome proliferator-activated receptor-alpha. J Neuroinflammation 9, 49. [PubMed: 22405189]

Sheng WS, Hu S, Hegg CC, Thayer SA, Peterson PK, 2000 Activation of Human Microglial Cells by HIV-1 gp41 and Tat Proteins. Clinical Immunology 96, 243–251. [PubMed: 10964543]

Singh IN, Goody RJ, Dean C, Ahmad NM, Lutz SE, Knapp PE, Nath A, Hauser KF, 2004 Apoptotic death of striatal neurons induced by human immunodeficiency virus-1 Tat and gp120: Differential involvement of caspase-3 and endonuclease G. J Neurovirol 10, 141–151. [PubMed: 15204919]

Speth C., Schabetsberger T., Mohsenipour I., Stockl G., Wurzner R., Stoiber H., Lass-Florl C., Dierich MP., 2002 Mechanism of human immunodeficiency virus-induced complement expression in astrocytes and neurons. J Virol 76, 3179–3188. [PubMed: 11884542]

Stella N, 2010 Cannabinoid and cannabinoid-like receptors in microglia, astrocytes, and astrocytomas. Glia 58, 1017–1030. [PubMed: 20468046]

Tchantchou F, Tucker LB, Fu AH, Bluett RJ, McCabe JT, Patel S, Zhang Y, 2014 The fatty acid amide hydrolase inhibitor PF-3845 promotes neuronal survival, attenuates inflammation and improves functional recovery in mice with traumatic brain injury. Neuropharmacology 85, 427–439. [PubMed: 24937045]

Tsou K, Brown S, Sanudo-Pena MC, Mackie K, Walker JM, 1998 Immunohistochemical distribution of cannabinoid CB1 receptors in the rat central nervous system. Neuroscience 83, 393–411. [PubMed: 9460749]

Vicente-Sanchez A, Sanchez-Blazquez P, Rodriguez-Munoz M, Garzon J, 2013 HINT1 protein cooperates with cannabinoid 1 receptor to negatively regulate glutamate NMDA receptor activity. Mol Brain 6, 42. [PubMed: 24093505]

Wallace DR, Dodson SL, Nath A, Booze RM, 2006 Delta opioid agonists attenuate TAT(1–72)-induced oxidative stress in SK-N-SH cells. Neurotoxicology 27, 101–107. [PubMed: 16168488]

Wang GJ, Chang L, Volkow ND, Telang F, Logan J, Ernst T, Fowler JS, 2004 Decreased brain dopaminergic transporters in HIV-associated dementia patients. Brain 127, 2452–2458. [PubMed: 15319273]

Wiebelhaus JM, Grim TW, Owens RA, Lazenka MF, Sim-Selley LJ, Abdullah RA., Niphakis MJ., Vann RE., Cravatt BF., Wiley JL., Negus SS., Lichtman AH., 2015 Delta9-tetrahydrocannabinol and endocannabinoid degradative enzyme inhibitors attenuate intracranial self-stimulation in mice. J Pharmacol Exp Ther 352, 195-207. [PubMed: 25398241]

Xu C, Hermes DJ, Mackie K, Lichtman AH, Ignatowska-Jankowska BM, Fitting S, 2016 Cannabinoids Occlude the HIV-1 Tat-Induced Decrease in GABAergic Neurotransmission in Prefrontal Cortex Slices. J Neuroimmune Pharmacol 11, 316–331. [PubMed: 26993829]

Xu C, Hermes DJ, Nwanguma B, Jacobs IR, Mackie K, Mukhopadhyay S, Lichtman AH, Ignatowska-Jankowska B, Fitting S, 2017 Endocannabinoids exert CB1 receptor-mediated neuroprotective effects in models of neuronal damage induced by HIV-1 Tat protein. Mol Cell Neurosci 83, 92–102. [PubMed: 28733129]

Zhang HY, Gao M, Shen H, Bi GH, Yang HJ, Liu QR, Wu J, Gardner EL, Bonci A, Xi ZX, 2016 Expression of functional cannabinoid CB2 receptor in VTA dopamine neurons in rats. Addict Biol.

Zou S, Fitting S, Hahn YK, Welch SP, El-Hage N, Hauser KF, Knapp PE, 2011 Morphine potentiates neurodegenerative effects of HIV-1 Tat through actions at mu-opioid receptor-expressing glia. Brain 134, 3616–3631. [PubMed: 22102648]

Zucchini S, Pittaluga A, Brocca-Cofano E, Summa M, Fabris M, De Michele R, Bonaccorsi A, Busatto G, Barbanti-Brodano G, Altavilla G, Verlengia G, Cifelli P, Corallini A, Caputo A, Simonato M, 2013 Increased excitability in tat-transgenic mice: role of tat in HIV-related neurological disorders. Neurobiol Dis 55, 110–119. [PubMed: 23454193]

Highlights

- Neuronal injury is a major component of HAND pathology.

- Endocannabinoid drugs show promise as a treatment for neurodegenerative disease.

- Assessment of cannabinoid based interventions in neuroAIDS is limited.

- FAAH inhibition blocks Tat induced neuronal dysfunction via cannabinoid receptors.
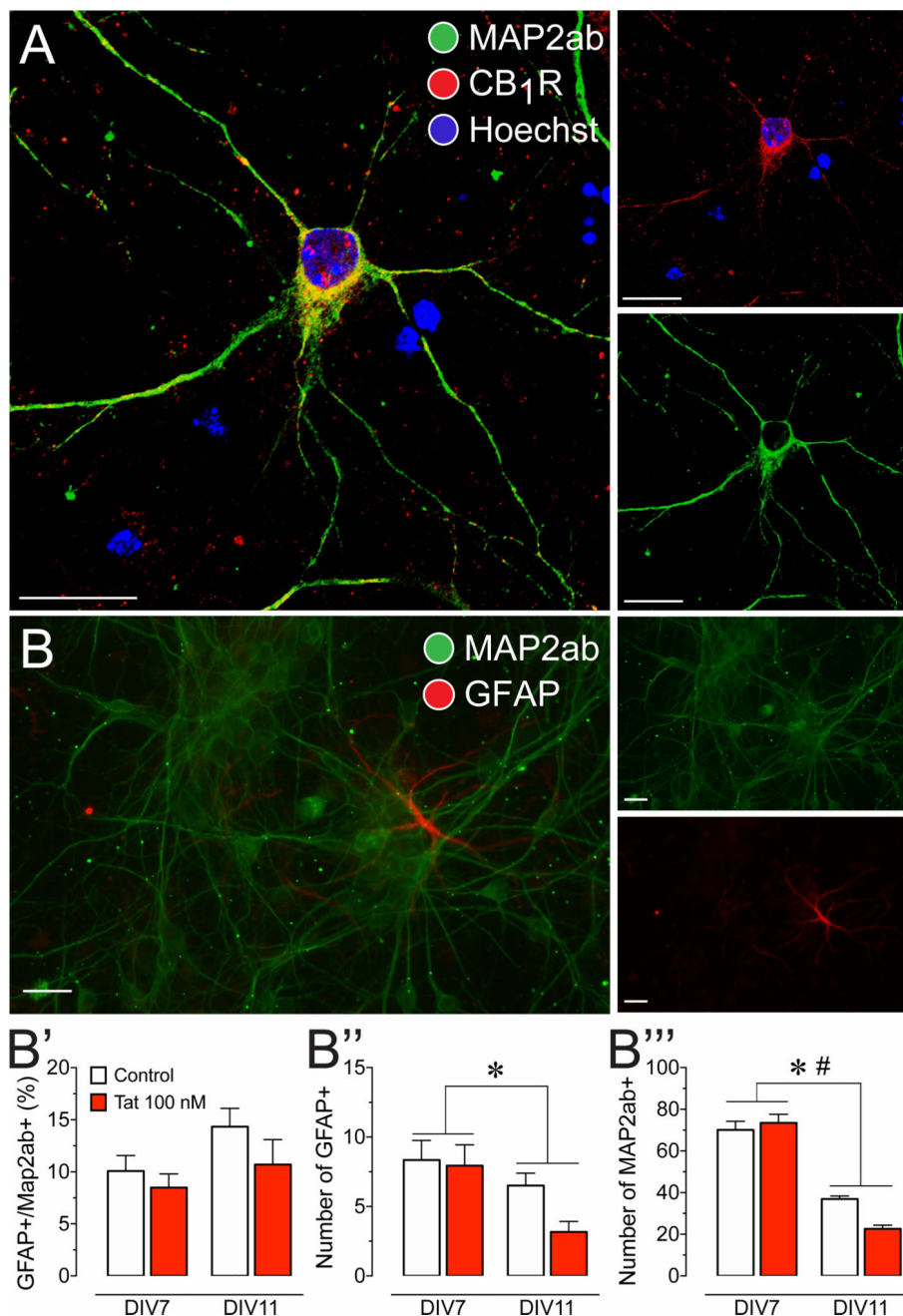
Figure 1. Presence of CB$_1$R in primary dissociated PFC neuronal cultures at day *in vitro* 7–11.
(A) Immunohistochemistry was conducted on PFC neurons (DIV 7–11) to identify cellular distribution of CB$_1$R. Cells were stained for Map2 (green) and endogenous CB$_1$R (red), and imaged using the Zeiss LSM 700 confocal microscope. CB$_1$R are localized in the soma and dendritic processes of PFC neurons, indicating that the cannabinoid machinery is present in our PFC primary cell culture model. (B) Immunohistochemistry was conducted on PFC neuronal cultures to calculate a ratio of glial cells to neurons. Cells were stained for Map2ab (green) and GFAP (red), and imaged using the Zeiss Axio Observer Z.1 microscope. (B')
GFAP-positive cells with astrocyte morphology were present in our PFC cultures and made

up about 11% of the cultured cells. The percent astroglia composition was not significantly altered by Tat 100 nM incubation and/or time (DIV 7–11). Independent assessment of astroglial (B") and neuronal (B'") populations revealed a significant reduction in both populations over 4 days *in vitro* (DIV 7–11). Further, for Map2ab-positive neuronal population a significant time by Tat interaction was noted that further decreased neuronal cell count. Statistical significance was assessed by two-way ANOVAs (at least three independent experiments), $*p < 0.05$ main effect of time, $\#p < 0.05$ time x Tat interaction. Scale bars = 20 μm.
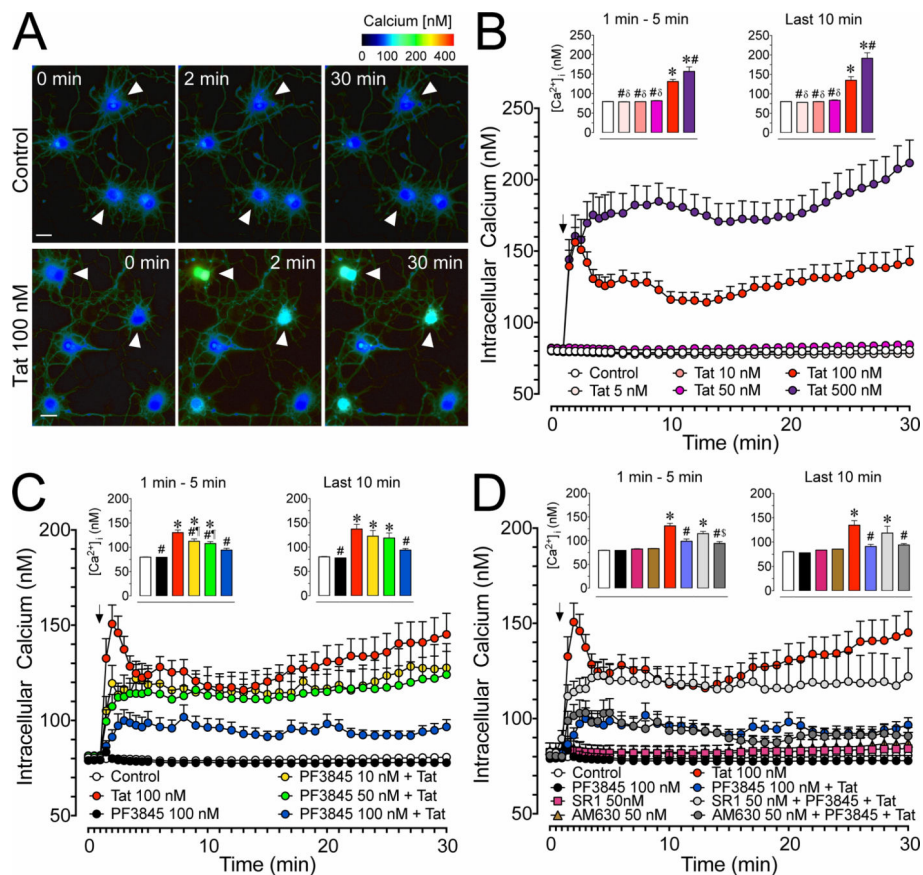
Figure 2. Calcium changes in cultured PFC neurons over 30 min.
(A) Pseudocolor images of control and Tat conditions assessing changes in $[Ca^{2+}]_i$ levels by ratiometric imaging of fura-2AM indicated minimal changes for control (white arrowheads, top row) but prominent changes for Tat 100 nM over a 30 min time period (white arrowheads, bottom row). (B) Significant Tat concentration dependent increases in $[Ca^{2+}]_i$ levels were noted over 30 min with Tat 100 nM and 500 nM being significantly different from control. (C) The significant increase in $[Ca^{2+}]_i$ levels by Tat 100 nM was significantly decreased by PF3845 pretreatment (10, 50, 100 nM) in a concentration-dependent manner (PF3845 pretreatment 30 min prior Tat application). (D) The protective effect of PF3845 100 nM pretreatment against Tat-induced increase in $[Ca^{2+}]_i$ levels was blocked by SR1 50 nM but not AM630 50 nM (CBR pretreatment 30 min prior PF3845 application). Statistical significance was assessed by ANOVAs followed by Bonferroni's post hoc tests; $*p < 0.05$ vs. control, $^\#p < 0.05$ vs. Tat 100 nM, $^\delta p < 0.001$ vs. Tat 500 nM, $^\P p < 0.05$ vs. PF3845 100 nM, $^\$p < 0.001$ vs. SR1 50 nM + PF3845 100 nM + Tat 100 nM (at least three independent experiments). SR1: SR141716A. Scale bars = 20 µm.
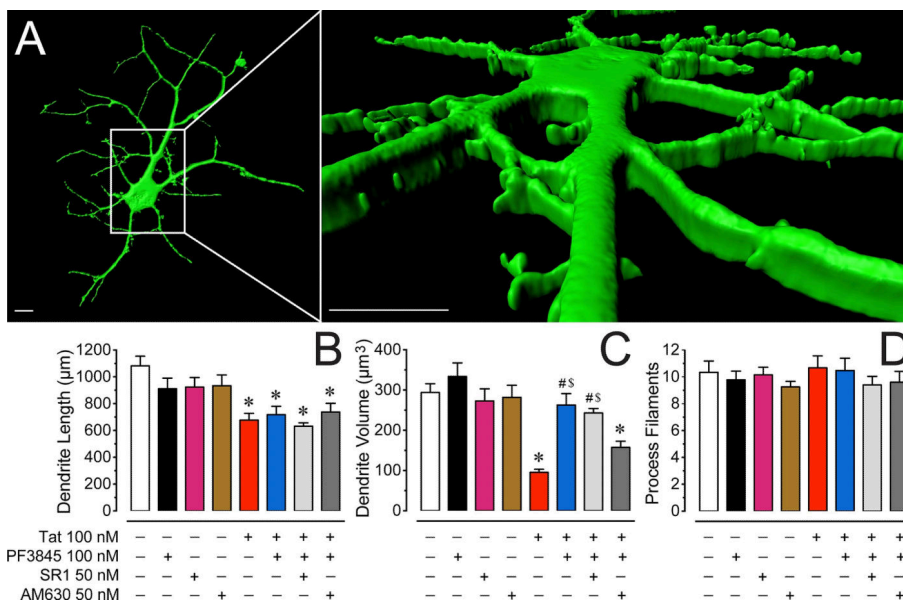
Figure 3. Morphological changes on dendrites of PFC neuronal cultures.
(A) Three-dimensional reconstruction of PFC neuronal dendrites at DIV 8 (B) Total
dendritic length (μm) is significantly decreased by Tat 100 nM after 24 h. No protective
effect was noted when pretreating Tat-exposed neurons with the FAAH enzyme inhibitor
PF3845 100 nM. (C) In contrast, the significant reduction of total dendritic volume (μm^3) by
Tat 100 nM was prevented with pretreatment of PF3845 100 nM. Interestingly, whereas SR1
50 nM was not able to block the protective effects of PF3845 100 nM, the CB$_2$R antagonist
AM630 50 nM reduced dendritic volume comparably to the Tat 100 nM treatment condition.
(D) The total number of process filaments were not significantly different between
conditions. Statistical significance was assessed by ANOVAs followed by Bonferroni's post
hoc tests; *$p < 0.01$ vs. control, #$p < 0.001$ vs. Tat 100 nM, $$p < 0.05$ vs. AM630 50 nM +
PF3845 100 nM + Tat 100 nM (at least three independent experiments). SR1: SR141716A.
Scale bars = 10 μm.

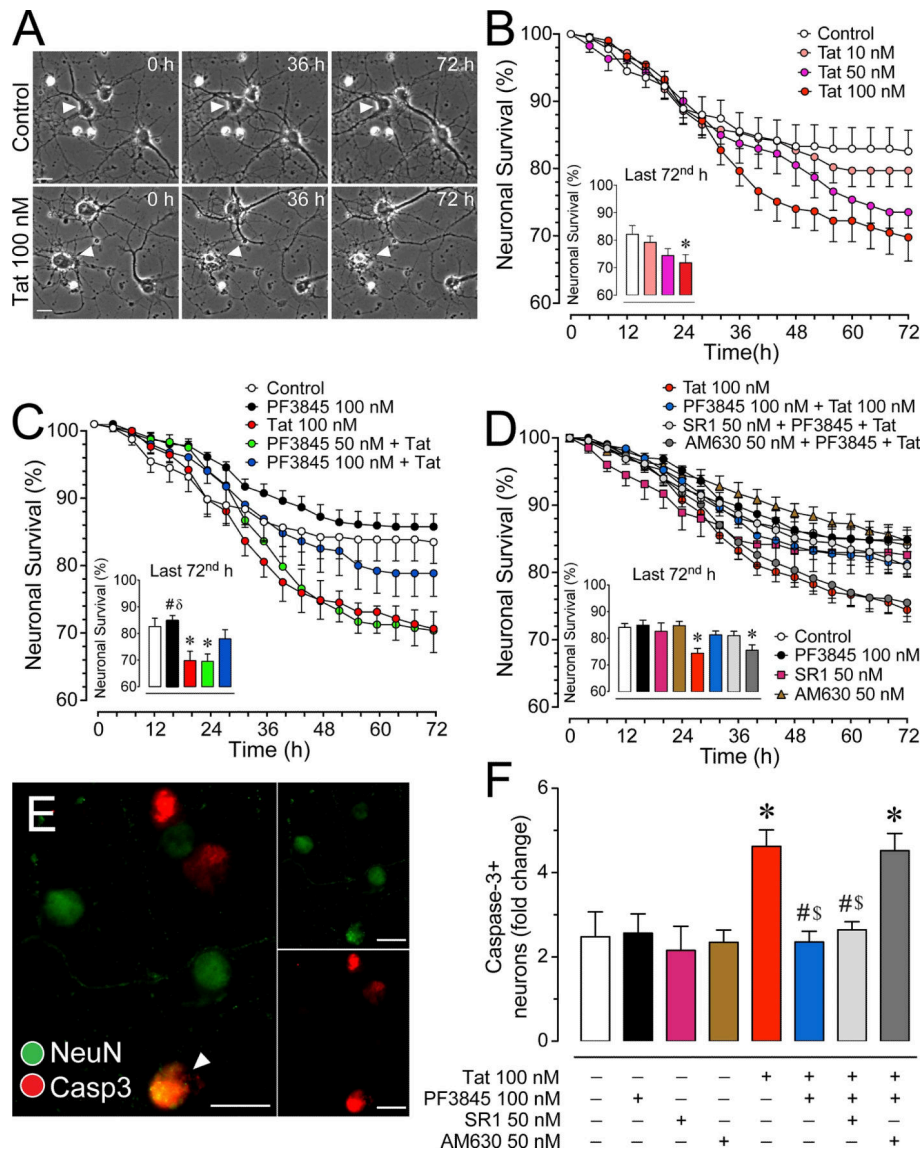**Figure 4. Changes in neuronal survival in cultured PFC neurons over 72 h.**
(A) Phase images of PFC neuronal cultures of control and Tat conditions assessing neuronal survival in a time-lapse study over a 72 h time period. A single neuron followed for the control condition shows neuronal survival over 72 h (white arrowheads, top row), whereas a single neuron followed after exposure to Tat 100 nM died at approximately 36 h (white arrowheads, bottom row) although other adjacent neurons remain alive and occasionally exhibit movement during this time period (white arrow, bottom row). (B) Treatment of Tat 100 nM for 72 h significantly reduced the survival of PFC neurons in a concentration-dependent manner, with Tat 100 nM being significantly different from control. (C) The significant decrease of neuronal survival by Tat 100 nM was significantly decreased by PF3845 100 nM pretreatment (30 min prior Tat application). (D) The protective effect of PF3845 100 nM pretreatment against Tat-induced increase in neuronal death was blocked by AM630 50 nM but not SR1 50 nM (CBR pretreatment 30 min prior PF3845 application). (E) Immunohistochemistry was conducted on PFC neuronal cultures to calculate the

proportion of activated caspase-3 (red) in NeuN-positive neurons (green) (white arrowhead, co-staining). Cells were imaged using the Zeiss Axio Observer Z.1 microscope. (F) A significant increase in caspase-3 positive neurons was noted for Tat 100 nM and AM630 50 nM + PF3845 100 nM + Tat 100 nM, suggesting that PF3845 protects neurons against Tat-induced neuronal injury and/or death through CB_2R related signaling. Statistical significance was assessed by ANOVAs followed by Bonferroni's post hoc tests; $*p < 0.05$ vs. control, $^{\#}p < 0.05$ vs. Tat 100 nM, $^{\delta}p < 0.05$ vs. PF3845 50 nM + Tat 100 nM, $^{\$}p < 0.05$ vs. AM630 50 nM + PF3845 100 nM + Tat 100 nM (at least three independent experiments). SR1: SR141716A, Casp3: active caspase-3. Scale bars = 20 μm.
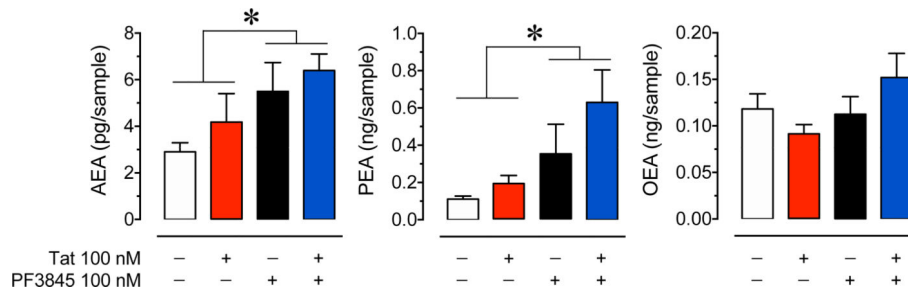
Figure 5. PF3845 mediated changes in endocannabinoid concentration in PFC neuron cultures.
Concentrations of AEA, PEA, and OEA were assessed using UPLC-MS/MS after 30 min of PF3845 100 nM ± Tat 100 nM exposure. Lipid concentrations were normalized to cell count for each independent experiment. A significant main effect of PF3845 treatment was detected for AEA and PEA. No significant differences were noted for OEA. Statistical significance was assessed by two-way ANOVAs; *$p < 0.05$ main effect of PF3845. Each condition represents at least three independent experiments.